Importance of drilling-related processes on the origin of borehole breakouts — Insights from LWD observations

Kai Stricker [a],[*], Stefan Schimschal [b], Birgit Müller [a], Stefan Wessling [b], Florian Bender [c], Thomas Kohl [a]

[a] *Institute of Applied Geosciences, Karlsruhe Institute of Technology (KIT), Kaiserstraße 12, 76131 Karlsruhe, Germany*
[b] *Baker Hughes, Baker-Hughes-Straße 1, 29221 Celle, Germany*
[c] *Baker Hughes, Ytrebygdsvegen 215, 5258 Bergen, Norway*

ARTICLE INFO

ABSTRACT

Logging while drilling (LWD) images are widely used for the analysis of borehole stability. In this context, borehole breakouts are a crucial indication of rock failure developing when the circumferential stress around the borehole exceeds the yield value of the rock. This study investigates the impact of drilling-related processes (DRPs) on the origin of borehole breakouts. DRPs, for instance, include connections or tripping operations. For this purpose, we analyze data from 12 boreholes in different geological settings throughout the Norwegian and Danish North Sea, containing a total of 208 borehole breakouts. The extensive data acquisition of LWD offers the unique possibility to link the imaging to real-time drilling operations and to monitor anomalies of e.g., bottom hole pressure. These records allow us to connect any thermal, hydraulic, or mechanical interaction next to the borehole wall to perturbations of the stress field. This analysis resulted in an apparent strong coincidence of borehole breakouts, representing major stress perturbations, with DRPs. The causal relationship is highlighted by one order of magnitude higher occurrence of DRPs in depth sections containing breakouts. Major pressure reductions in the annulus of the borehole seem to be the most significant cause of drilling-related wellbore failures. This applies in particular to shutting off the pumps during connections, where pressure reductions of up to 16 % of the annulus pressure led to higher circumferential stresses. This process will increase the likelihood of compressive and shear failure, therefore causing borehole breakouts. These observations further open the perspective of counteracting wellbore instabilities by pressure modification. In addition to the initiation of breakouts, their temporal evolution – as seen in relogs – can also be ascribed to DRPs. This study indicates that not only plasticity but also mechanical interaction from DRPs is a key driver of the temporal growth of borehole breakouts.

1. Introduction

In drilling operations, wellbore stability is crucial for preserving the drilling investments.[1–4] In a given stress field, possible wellbore instabilities are typically due to low rock strength resulting in compressive borehole breakouts, which potentially lead to the collapse of the borehole.[5] Using image logs, the orientation of the stress components[6–8] and the stress magnitude around wellbores[5,9,10] are determined. Borehole instabilities can further be used to derive characteristic geomechanical parameters for reservoir models.[5] In the past, they have been monitored mostly by wireline logging[8,11,12], whereas recently, logging while drilling (LWD) tools are gaining more importance.[2,13–15]

Borehole breakouts develop when concentrations of the circumferential stress around the borehole exceed the yield value of the rock. Their average orientation corresponds to the minimum stress component S_{min}. In contrast, tensile fractures (e.g. hydraulic fractures or so-called drilling-induced fractures (DIFs)) originate from the drilling process and are caused when the circumferential stress falls below the tensile strength of the rock.[5,16] They are oriented in the direction of the maximum stress component, S_{max}. The azimuthal orientation and inclination of a borehole in the subsurface additionally influence the circumferential stress state and thus the development of both, breakouts and tensile fractures.[17] Besides their geological origin – thus as a consequence of high tectonic differential stresses, they may be caused through drilling operations.[18–20] Mechanical erosion by reciprocation or rotation of the drill string or hydraulic pressure through

* Corresponding author.
E-mail addresses: kai.stricker@kit.edu (K. Stricker), stefan.schimschal@bakerhughes.com (S. Schimschal), birgit.mueller@kit.edu (B. Müller), stefan.wessling@bakerhughes.com (S. Wessling), florian.bender@bakerhughes.com (F. Bender), thomas.kohl@kit.edu (T. Kohl).

excessive mud circulation are typical sources that yield stress concentrations locally exceeding the yield value of the rock.[21] Also, an inappropriate selection of the mud weight may induce borehole instabilities when the pressure level cannot be kept in the window defined by collapse and fracture pressure.[19,22] Throughout this paper, we will refer to all compressive borehole failure phenomena as "borehole breakouts". This includes borehole breakouts occurring in areas with extensive reaming or circulation.

While the physical principles for the occurrence of borehole breakouts are mathematically well described, their temporal development remains controversial. Whereas Zoback (2007)[5] states that breakouts tend to deepen over time but generally show no increase in width, other studies describe a temporal growth of breakouts in all dimensions.[23,24] Advances in technologies, such as enhanced digital communication between bit and surface or recent improvements in LWD measurements (e.g. high-resolution LWD images) are now opening the pathway for real-time wellbore stability services.[15] Especially, it is now possible to investigate the dynamic processes in a borehole and to combine multiple types of LWD datasets with drilling-related processes (DRPs).

Today modern LWD techniques enable the combined evaluation of formation imaging with operational drilling data. In this paper, we utilize the extensive data acquisition of LWD to expand the standard interpretation of borehole breakouts, as being the result of heterogeneities in stress state and rock strength, towards the impact of DRPs. This innovative approach leads to new data analysis methods that allow for the differentiation between drilling-induced breakouts and breakouts of purely geological origin. We analyze LWD image logs and their relog sections (image recordings during tripping procedures) as well as other real-time measured drilling-related parameters (such as the mud pressure) by extending standard industry application tools to improve the general understanding of the origin of breakouts. Next, the impact of DRPs on the dynamic hydraulic conditions in the borehole and their implications on the origin of breakouts is investigated. Finally, relog sections and recordings of multiple imaging tools are analyzed to investigate the time-dependent behavior of breakouts. Conclusively, this should deepen the understanding of the influence of DRPs on the development of breakouts and open the perspective of adapting drilling operations to counteract wellbore instabilities.

2. Background information

2.1. Geomechanical models around boreholes

Failure of rock depends on the effective stress and is well described in literature on rock mechanics (e.g. Refs. 5, 25) . The Mohr circle illustrates the relationship between the failure of rock and the stress state (Fig. 1). The yield envelope indicates the limit of elasticity, beyond which permanent deformations occur. At low confining pressures, the yield envelope can be interpreted as a failure threshold. Various failure criteria are described in literature (e.g. Ref. 26), a detailed consideration of these criteria is beyond the scope of this study. The increase of pore pressure leads to a reduction of the effective stress and consequently to a stress state closer to failure.[25]

In a far-field stress field, the removal of material through the drilling process leads to a stress concentration around the borehole.[5,27] When the maximum magnitude of effective circumferential stress $\sigma_{\theta\theta,eff}^{max}$ exceeds the yield value, borehole breakouts will occur at this orientation. At the wall of a vertical borehole where the normal vertical stress is one of the principal stresses, $\sigma_{\theta\theta,eff}^{max}$ is parallel to the minimum principal horizontal stress, S_h, and is given by

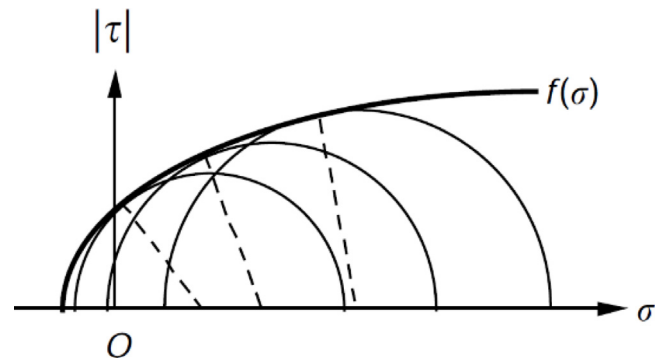$$\sigma_{\theta\theta,eff}^{max} = 3S_H - S_h - 2P_0 - \Delta P - \sigma^{\Delta T} \tag{1}$$

Fig. 1. Mohr circles with yield envelope (or failure curve) $f(\sigma)$ defining the limit of elasticity, beyond which permanent deformations (or failure for low confining pressure) occur. σ is the stress normal to the failure plane. τ is the shear stress on the failure plane.
Source: Adapted from Ref. 25.

Where S_H is the maximum principal horizontal stress, P_0 the pore pressure of the formation, ΔP the difference between the wellbore pressure and the formation pore pressure, and $\sigma^{\Delta T}$ the thermal stress caused by the temperature difference between drilling mud and formation.[5]

Assuming a given stress state, it becomes clear that the variation of the pressure in the wellbore affects $\sigma_{\theta\theta,eff}^{max}$ and thus the stability of the wellbore. A pressure decrease in the wellbore (resulting in a decrease of ΔP) increases $\sigma_{\theta\theta,eff}^{max}$ and can lead to the occurrence of breakouts. In contrast, a pressure increase decreases the effective circumferential stress, potentially leading to tensional failure.[5] Even though the calculation of the circumferential stress for inclined boreholes is slightly more complex (see Ref. 17), the effect of changes in the wellbore pressure are comparable to vertical boreholes.

In standard breakout models, changes in the circumferential stress around the borehole are considered for the initial development of breakouts (e.g. Ref. 5). These static models neglect dynamic changes. However, in other disciplines, the dynamic impact on pressure/stress changes is well-known e.g. for water hammering in pipes[28] or during blasting excavation in tunnels (e.g. Ref. 29). For the latter, blast loading and transient unloading lead to strong dynamic stress fluctuations in the range of milliseconds that finally lead to the failure of the rock.[29] We may consider this recurring influence as being an approximate analog of the short-time-scale pressure perturbations occurring during DRPs, which lead to dynamic changes in the effective circumferential stress.

2.2. Drilling-related processes and logging while drilling (LWD) borehole measurements

Various processes are necessary for a smooth continuation of a drilling operation, including connections and different variations of pipe trips.[30] These processes can cause thermal, hydraulic, and mechanical loads on the rock surrounding the borehole, potentially leading to conditions that are favorable for borehole instabilities. In this section, we will shortly review how these perturbations may impact the mechanical stability of the rock, especially at the bottom of the borehole (e.g. Ref. 31). Both the execution of connections (i.e. stop pumping down hole[30] and tripping operations (pulling the drill string out of the borehole[32]) lead to pressure reductions (swab pressures) within the annulus of the borehole. This further leads to an increase in the effective circumferential stress around the borehole wall[5]; consequently, borehole breakouts may occur if the yield value at the borehole

Table 1

Overview of the analyzed data in this study (confidential data was omitted). All data is older than two years and thus available on the Diskos Well Database of the Norwegian Petroleum Directorate.[35] Non-confidential analyzed data has been made available in an online repository.[36]

Field name	Well name	Depth extent (MD) [m]	Inclination [°]	Analyzed logs	Sources for geology and geomechanics
Oseberg	30/6-E-5 B	3647–6259	65.7–90.0	ACL, DEN, CAL, P, T	Refs. 37, 38
	30/6-E-8 A	3490–5837	63.4–90.0	ACL, DEN, CAL, P, T	
	30/6-H-2	2741–4022	54.3–88.4	ACL, ACH, DEN, CAL, P, T	
	30/6-H-8 AY1	3308–4219	81.2–90.0	ACL, DEN, CAL, P, T	
	30/9-B-11 B	5170–6149	69.7–90.0	ACL, DEN, CAL, P, T	
	30/9-F-17 CT2	4800–5531	74.5–90.0	ACL, DEN, CAL, P, T	
Rolvsnes	16/1-28 S	3244–4782	86.8–90.0	ACL, DEN, CAL, P, T	Ref. 39
Troll	31/2-L-22	2001–4805	88.0–90.0	ACL, DEN, CAL, P, T	Refs. 37, 40, 41
	31/2-N-22	2151–4345	88.0–90.0	ACL, DEN, CAL, P, T	
Valhall	2/8-G-17	3459–5289	84.1–90.0	ACL, ACH, DEN, CAL, P, T	Refs. 42–44

wall is exceeded by this stress.[16] On the contrary, lowering the drill string too fast into the hole leads to significant pressure increases (surging effect[33]). This decreases the effective circumferential stress around the borehole, facilitating the generation of tensile fractures if this stress drops below the tensile strength of the rock.[5] In addition to their influence on hydraulic conditions within a borehole, tripping operations also exert mechanical loads on boreholes and may affect their stability. They are frequently part of so-called reaming operations to clean a borehole, e.g. before a connection, and are reported to have a direct (negative) influence on the wellbore stability.[31,34]

In contrast to wireline logging, which relies mainly on gravity to run the device into the borehole, LWD measurements can be easily utilized in inclined or horizontal boreholes with complex geometries. The LWD tools are installed within drill collars at the lowermost part of the drill string and allow the real-time quantification of perturbations (e.g. pressure) while drilling as well as their impact on wellbore stability.[45] The acquisition timing of LWD is the central advantage compared to wireline logging[46], opening the pathway to investigate the relationship between DRPs and borehole breakouts.

Among other measurements, LWD tools can be used to record an image of the wellbore wall by measuring different physical properties. This includes, for instance, acoustic, density, and electrical images.[47] Acoustic image logs are based on the reflection of acoustic signals from the borehole wall, allowing to record both the amplitude and the travel time of these signals with a large bandwidth of possible applications.[48] Density image logs rely on the scattering of Gamma rays that are sent into the formation depending on the density thereof. Borehole enlargements become apparent through measurement values below the expected bulk density due to increased drilling fluid fraction in the measured sample volume.[49] Electrical image logs enable the measurement of the shape of the borehole wall based on the resistivity contrast between the drilling mud and the formation surrounding the borehole. The shallow depth of investigation of ca. 0.5 in for modern LWD tools allows for a detailed shape determination of borehole enlargements.[47,50]

2.3. Data and methods

2.3.1. Data overview

The data sets used for this study were acquired in multiple geological settings throughout the Norwegian and Danish North Sea.[51] In total, we analyzed data originating from 12 boreholes located in six hydrocarbon fields with varying inclinations, mostly either strongly inclined or horizontal (Table 1). The data comprise various image log types that range from electrical, over density, to low- and high-resolution acoustic images. Furthermore, supplementary information from caliper, pressure, and temperature

logs were utilized. Table 1 gives an overview of the used logs for each investigated borehole.

Most of the data originate from the reservoir level of the respective wells. Logs acquired in the Northern Viking Graben cover thinly laminated mud rocks of the Late Jurassic age Heather Formation and interbedded sandstone, paleosol, and coal intervals of the Middle Jurassic Brent Group (Oseberg Field). On the Horda Platform, image logs originate from Middle to Late Jurassic tide-dominated delta sandstone sequences (Troll Field). Data from the Central Graben and the Norwegian-Danish Basin are mainly acquired in chalk carbonates of the Late Cretaceous age (Valhall Field). To extend the variety of lithofacies covered, additional data from in-situ and weathered magmatic basements were used (Rolvsnes Field).[52] All formations within the sedimentary sequence are situated in a normal faulting environment, close to isotropic stresses.[53] The stress regime in the basement is assumed to be unrelated to that in the sedimentary sequence.[54] References to the geology and the geomechanics of the hydrocarbon fields are provided in Table 1.

2.3.2. Analysis concept

To evaluate the relationship between breakouts and DRPs, multiple image log types (acoustic, density, and electrical) are used to identify breakouts. The identification of the breakouts and the discrimination of them from other deformations has been performed according to prior research on this topic.[8,15,55] The analysis of caliper logs further supports the selection of breakouts. The occurrence and frequency of DRPs and their relationship to the origin of borehole breakouts are analyzed under the application of different methods. First, the frequency of occurrence of DRPs is determined for all selected breakouts, and subdivided into pump shut-off events (e.g. connections) as well as minor (<5 m) and major (>5 m) tripping operations. Afterward, the frequency of occurrence of tripping operations and pump shut-off events within and outside of breakout sections is compared. Further, mud pressure anomalies in the wellbore are analyzed due to their strong influence on the effective circumferential stress at the borehole wall. This may impact the wellbore stability, e.g., when the effective circumferential stress exceeds the yield value of the rock. The described procedure was applied to the borehole image, supplementary caliper, and pressure data that was obtained from 12 boreholes located in six hydrocarbon fields.

In the case image relog data (data recorded over the same depth interval, but at later times during tripping operations) are available for the respective borehole breakout, potential temporal geometrical changes, as described in Ref. 5, can be analyzed. These time-dependent changes of breakouts were additionally used for the identification of a relationship between the breakout occurrence and the performed DRPs during this time frame.
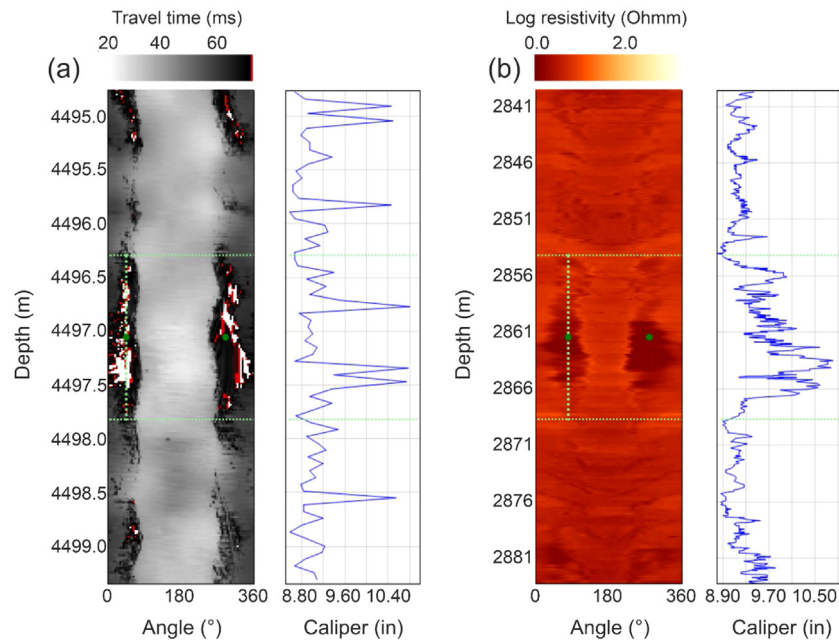
Fig. 2. Examples of breakouts that were identified in a high-resolution (256-sector) LWD ultrasonic image obtained from well 2/8 − G − 17 in the Valhall field on the Norwegian continental shelf (a) and an electrical image obtained from the Valdemar field on the Danish continental shelf (b). The identification of the breakouts was aided by the recomputed average caliper log (blue curves). The horizontal dashed green lines indicate the vertical extent of each breakout, whereas the filled green circles mark the orientation of the two opposed parts of the respective breakout.. (For interpretation of the references to color in this figure legend, the reader is referred to the web version of this article.)

3. Results

3.1. Observed borehole instabilities

In the investigated data sets breakouts occur frequently. In total, 208 breakout sections were identified. Detailed information on their location (i.e. the well they have been identified in) and their geometry (i.e. their depth, length, or orientation) is provided in the supplementary material of this study.[36] Fig. 2 shows examples of breakout sections that were identified in a high-resolution ultrasonic image (Fig. 2a) and a high-resolution electrical image (Fig. 2b).

Various other borehole instabilities can be observed in the investigated datasets. Frequently, breakout sections contain superimpositions of a breakout and an additional borehole enlargement, which e.g. occurs along a bedding plane. This kind of superimposition occurs for a third of all breakout sections (70 out of 208) and is mostly related to beds with a lower density than the surrounding rock. Reasons for these enlargements comprise generally unstable formations, shales that are prone to roof collapse due to reduced arch support, or sloughing. Thus, in such formations, the origin of borehole breakouts may be further linked to the respective bedding structure, leading to failure structures with a broader azimuthal extent. Very rarely breakouts are superimposed by borehole enlargements that extend over the complete azimuthal section of the well (i.e. washouts) or with the scraping of the bit on either the low (probably a key seat) or the top side of the borehole. All mentioned instability phenomena are not limited to a superimposition with breakouts but can also occur individually. In conclusion, however, most investigated breakout sections (138 out of 208) seem to be unrelated to a specific lithology or other geological reasons.

3.2. Relationship between drilling-related processes and borehole breakouts

The investigated data, comprising 208 identified breakouts in 16 runs of 12 different boreholes, is impacted by a large number

of the before-described DRPs. The analysis of the data shows that 190 out of 208 breakouts are associated with one or more of these processes. This is illustrated by the gray bar in Fig. 3a. Conversely, this means that only 18 breakouts (or ca. 10 % of the investigated data) occur without any relation to drilling procedures and are most likely caused by the stress state around the borehole. With only one exception, drilling-controlled breakout sections are always accompanied by at least one pump shut-off event (red bar in Fig. 3a). This can be expected as connections need to be performed to continue the drilling operation. In addition to pump shut-offs, minor tripping events (<5 m; green bar), without any relation to connections, and major tripping events (>5 m; blue bar), such as wiper trips, are present in ca. 30 % of the investigated breakouts.

Fig. 3b shows the frequency histogram of all DRPs occurring during the investigated breakout sections. Moreover, the number of pump shut-off events (Fig. 3c), minor (Fig. 3d), and major (Fig. 3e) tripping operations are displayed. The color of the histograms corresponds to the respective bars in Fig. 3a; the x-axes of all histograms are further limited to a maximum of ten processes per breakout for better visibility. Fig. 3b illustrates the frequency distribution of all DRPs occurring during drilling-controlled breakout sections that are associated with at least one DRP. The vast majority (148) of these breakouts are related to less than five DRPs, whereas only a smaller amount of these breakout sections (31) is affected by up to ten DRPs. Breakouts that are related to more than ten DRPs are even scarcer (not displayed in the figure).

Breakout sections that comprise a relation to one or two DRPs are mostly related to pump shut-off events during connections, which are regularly performed while drilling (i.e. adding new stands of drill pipe to the drill string). This is underpinned by the frequency distribution of pump shut-off events displayed in Fig. 3c, showing that 156 out of 190 drilling-controlled breakout sections contain one or two pump shut-off events. Consequently, breakout sections comprising more than one or two DRPs are very likely additionally influenced by tripping operations. Fig. 3d and
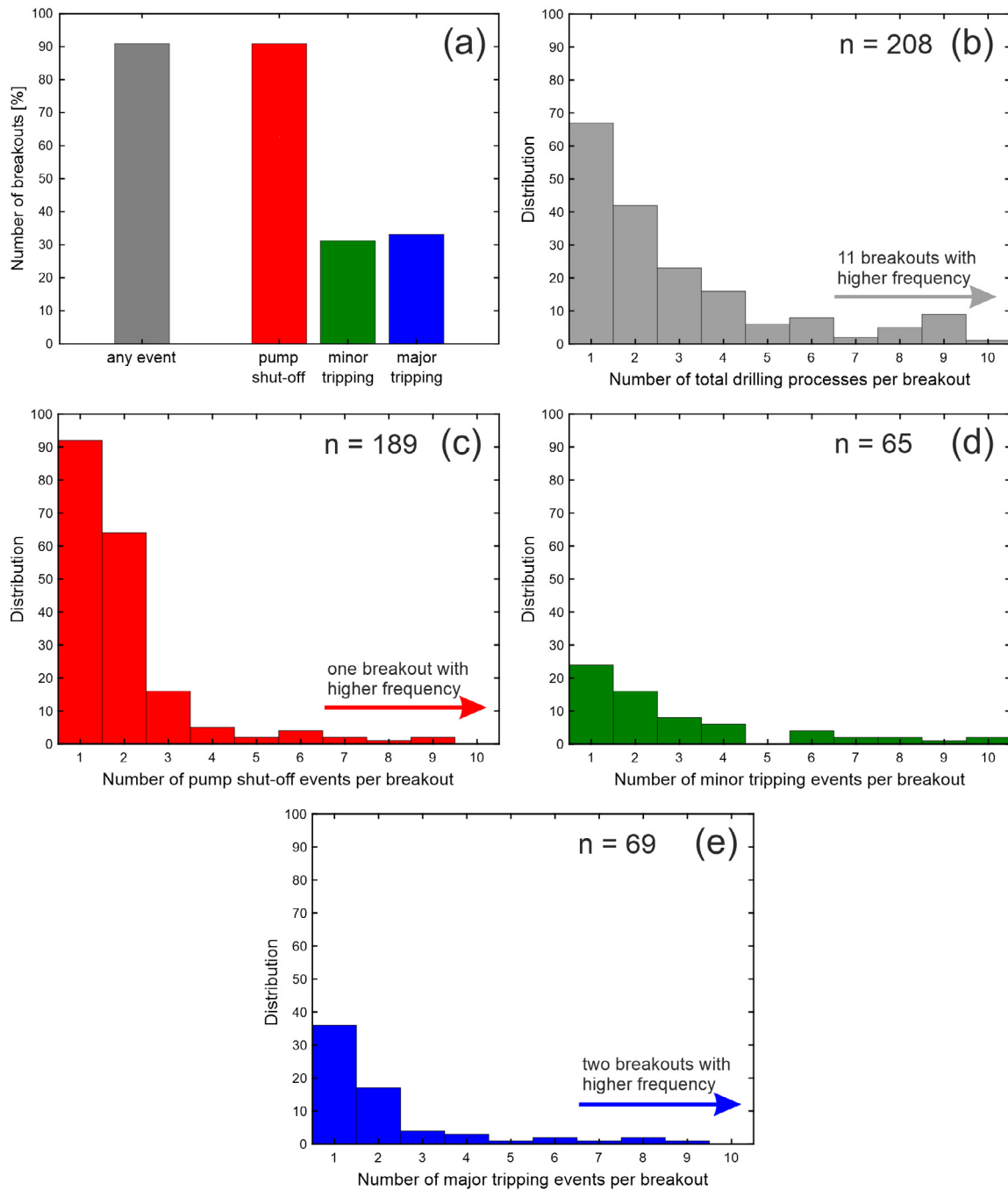
Fig. 3. Relationships between borehole breakouts and drilling-related processes (DRPs). (a) Number of breakouts associated with any DRP (gray) as well as pump shut-off events (red), minor (<5 m; green), and major tripping events (>5 m, blue). Distribution of the frequency of occurrence of the total amount of DRPs (b), pump shut-off events (c) as well as minor (d) and major (e) tripping events. (For interpretation of the references to color in this figure legend, the reader is referred to the web version of this article.)

3e show the frequency distributions of minor and major tripping operations, respectively. The frequency distributions show that most breakouts that are related to tripping operations only include a relatively low number of these operations. However, minor tripping operations tend to occur more frequently with higher absolute numbers, than their major counterpart does.

In the next step, we compared the frequency of occurrence of tripping operations and pump shut-off events within and outside of breakout sections. The intention was to improve our understanding of the relationship between the drilling procedure and breakouts. For tripping operations, this analysis has been limited to major trips with a length of more than five meters.

It can be shown that both tripping operations and pump shut-off events occur significantly more frequently within breakout sections than outside. Tripping operations tend to occur by one order of magnitude more frequently within breakout sections than outside of these sections (9.27 compared to 0.92 tripping operations per 100 m measured depth (MD)). Similarly, pump shut-off events (e.g. connections) are also significantly more common within breakout intervals than outside (0.16 compared to 0.03 events per m MD). This illustrates that in depth intervals with breakouts more DRPs, which are not necessarily related to the normal drilling procedure, were performed. In addition, it can be stated that either these DRPs contribute to the causation of
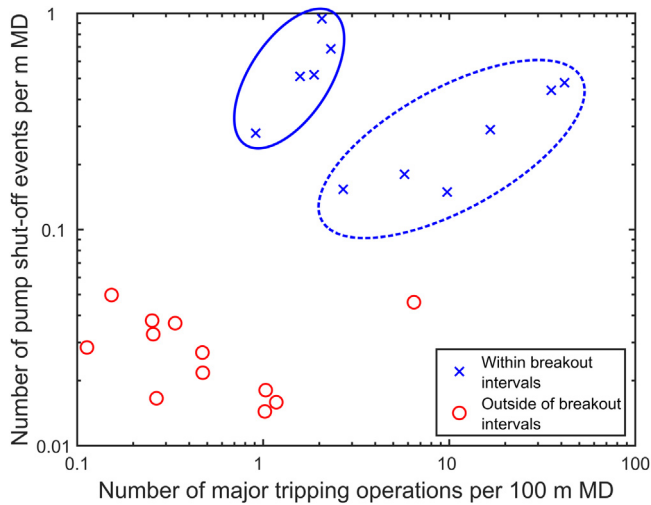
Fig. 4. Relationship between major tripping operations and pump shut-off events for different wells. Both processes occur more frequently within breakout sections (blue) than outside (red), pointing at a potential causal relationship. The data related to the breakout sections shows an increasing trend between the two processes, whereas outside of breakouts no trend is visible. (For interpretation of the references to color in this figure legend, the reader is referred to the web version of this article.)

Fig. 5. Normalized distributions of observed pressure reduction mechanisms during breakout sections: Swab pressures related to tripping operations (blue), pump shut-off events (primarily related to connections; red), and downlinks (green). All histograms are normalized to the total number of occurrences. The pressure reductions displayed in the histograms range from 0.1 to 6.5 MPa. (For interpretation of the references to color in this figure legend, the reader is referred to the web version of this article.)

breakouts or that their execution is a reaction to the breakout occurrence.

The increased frequency of occurrence of tripping operations and pump shut-off events within breakout sections can be further identified within a cross-plot (Fig. 4). The data are sorted by the wells they are originating from. The frequency of tripping operations and pump shut-off events for each well is represented by one marker for depths within breakouts (blue crosses) and outside of breakouts (red circles), respectively. The separation between the frequency of the two processes within breakout sections and outside of these is clearly visible, further pointing to a causal relationship between DRPs and the development of breakouts. Outside of breakout sections, both tripping operations and pump shut-off events occur very infrequently (except for one outlier) and show no clear relationship between the two parameters. Within breakout sections, however, the investigated data shows a linear trend between pump shut-off events and related major tripping operations. This means that individual trips were accompanied by a multitude of pump shut-off events, indicating a high likelihood that the breakouts in the respective wells were caused or enhanced by the interaction with these processes. This interpretation, however, is solely based on the statistical relationship between pump shut-off events and related major tripping operations. This means that as no individual breakouts were analyzed here, the actual stress state of the rocks surrounding the borehole, i.e. how close they already were to failure without the influence of the DRPs, was not considered.

3.3. Impact of drilling-related processes on borehole hydraulics

A multitude of negative pressure anomalies, which deviate from the hydrostatic pressure profile, were observed in the investigated breakout sections. Additionally, some positive pressure anomalies occur as well. The most prominent pressure variations are linked to connections (89 occurrences), tripping operations (74 occurrences), or other periods with shut-off pumps (21 occurrences). The pressure variations related to connections do not only comprise pressure decreases, initiated by the pumps shut-off during the connection itself but also generate smaller pressure
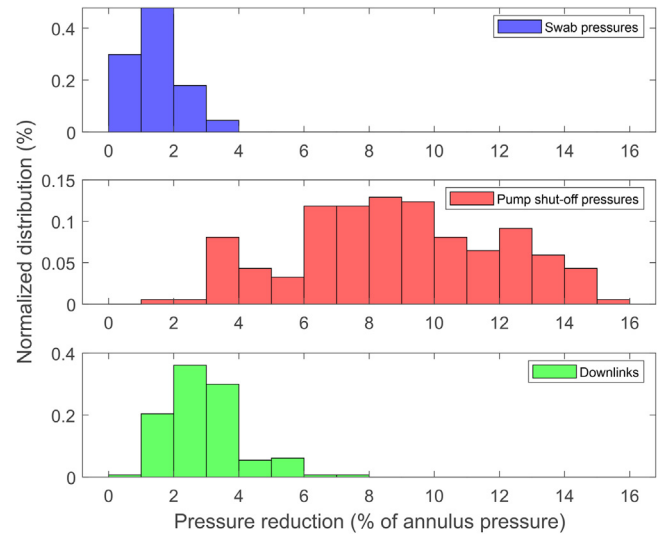
decreases after the pumps are switched on again. In total, about two-thirds of all investigated breakout sections (139 out of 208) comprise at least one negative pressure anomaly related to these processes. Furthermore, additional negative pressure anomalies related to downlinks, i.e. communication between the surface and the tools in the bottom hole assembly (BHA), could be observed in about a third of all breakout sections (61 out of 208). This means that most of the investigated breakouts contain reductions in the annulus pressure that are related to the drilling procedure and may contribute to the development of breakouts.

The observed pressure reductions are not only caused by different types of DRPs but also vary strongly in their magnitudes. Fig. 5 illustrates the normalized distributions of pressure reductions related to swab pressures, downlinks, and pump shut-off events. To minimize the influence of depth changes on the data (i.e. increasing hydrostatic pressure with depth), the histograms displayed in Fig. 5 show the distribution of the pressure reductions normalized to the average annulus pressure of the respective breakout section. Both, swab pressures and pressure reductions related to downlinks, vary in the range of 0 – 2 MPa, reaching up to four and eight percent of the average annulus pressure, respectively. Pump shut-off pressures comprise a broader range and reach much higher reductions of up to 6.5 MPa or 16% of the average annulus pressure. Such pressure reductions have a strong impact on the effective circumferential stress around the borehole, increasing it significantly. This enhances the likelihood of rock failure (e.g. breakouts) as the effective circumferential stress may exceed the yield value of the rock (Peška and Zoback 1995[5]). Hence, the high sensitivity of the annulus pressure and consequently also the effective circumferential stress on e.g. swab pressures[20] or pump shut-off events[56] have been investigated by various numerical studies.

Fig. 6 illustrates the relation between pressure drop anomalies and DRPs during an exemplary breakout section. Fig. 6a shows the MD of the drill bit (blue) and the image tool sensor (red) as a function of time. The deviations from a monotonous increase are caused by various pump shut-off events (P) and tripping operations (T). Fig. 6b shows the corresponding anomalies in
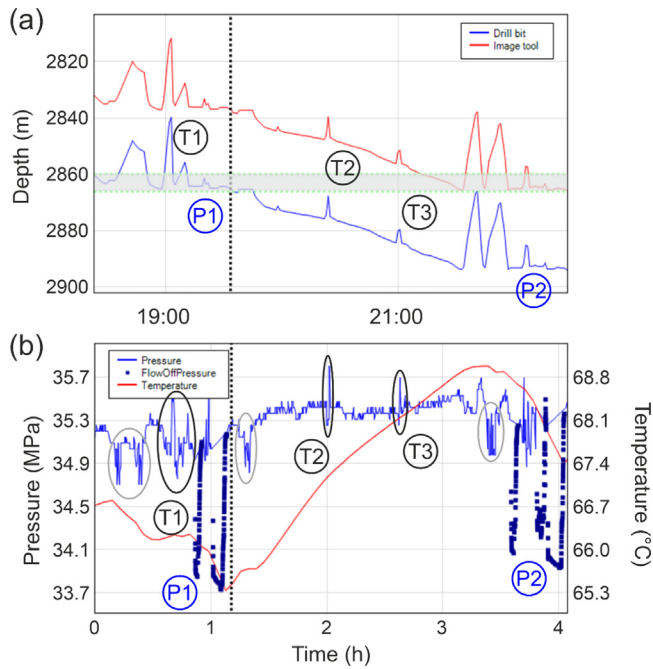
Fig. 6. Relationship between pressure anomalies and various drilling-related processes (DRPs) for an exemplary breakout section (the gray bar in (a) highlights its depth extent). (a) Bias between the occurrence of the breakout at the drill bit (blue) and detection at the image sensor (red), 27 m apart. (b) Pressure and temperature values recorded next to the drill bit in the breakout section. The labels T1, T2, and T3 mark different tripping operations (highlighted by black ovals in (b)); whereas the labels P1 and P2 mark two pump shut-off events. The labels apply both to variations in the depth of the drill bit and the image tool sensor (a) and their respective influences on pressure and temperature (b). Gray ovals further highlight pressure decreases that are related to downlinks. The displayed data originate from the Valdemar field in the Danish continental shelf. (For interpretation of the references to color in this figure legend, the reader is referred to the web version of this article.)

Fig. 7. Original image log (left) with a breakout section between 2860–2866 m and two relogs of the same depth interval illustrating breakout growth over time. Relog 1 (center) was recorded 112 min after the original log, whereas relog 2 (right) was recorded shortly afterward at a time lag of 124 min.

pressure and temperature caused by these DRPs. It is depicted that tripping operations (e.g. T1 – T3) often cause a rather slow pressure decrease, followed by a very sharp increase in pressure (black ovals). These pressure variation patterns can be attributed to swabbing and surging pressures. Connections (or generally pump shut-off events) are associated with the strongest pressure reductions (dotted blue lines). Their magnitude of ca. 1.5 MPa for this example is seven times larger than the pressure reductions related to tripping operations (0.2 MPa). Both examples in Fig. 6 (P1 and P2) are additionally accompanied by minor tripping operations and multiple additional pump shut-off events.

Gray ovals highlight additional pressure reductions that are related to downlinks. The first and third downlink overlap with tripping operations that precede a connection. This can be explained by the communication of the team at the surface of the rig with the tools in the BHA preceding a connection, potentially during a reaming procedure. In contrast, the second downlink follows the completion of a connection. Tripping operation T1 may represent a reaming procedure occurring directly before connection P1. Here, in addition to the hydraulic influence caused by the pressure reduction, lateral mechanical forces are applied to the wellbore wall, potentially leading to both ductile and brittle failure of the rocks surrounding the borehole.[57]

3.4. Time-dependent borehole instabilities

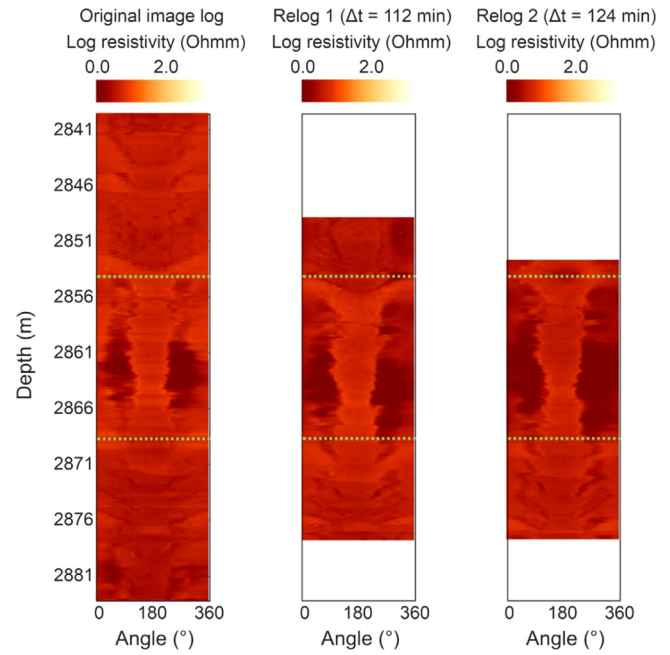In addition to the investigation of DRPs, LWD further offers the advantage of evaluating the mechanical development at logged sections. Here, we show the evolution of the resistivity image during relogs of the same depth interval. Fig. 7 illustrates such a development with an associated breakout growth during drilling, both in the azimuthal and in the MD direction. We compare the initial image to relog 1 recorded 112 min and relog 2 recorded 124 min after the logging of the respective depth section has taken place. Growth in breakout length and the opening angle is visible, even for the relatively small period between the two relogs.

Fig. 7 exposes a primary growth of the breakouts in length to be ca. 2.5 m downwards and ca. 5 m upwards from an initial length of ca. 6 m. In the azimuthal direction, the growth is also visible with relog widths of up to 165° from initially 118°. Such observation adds to earlier analyses of azimuthal growth. As such, Zoback (2007)[5] distinguishes between stable wells with initial breakout widths of less than 60° and unstable wells that are prone to temporal growth and subsequently increase the risk of failure due to their high initial breakout width of P more than 90°. In this context, our observation resembles the second type of breakouts.

4. Discussion

4.1. Breakouts originating from dynamic borehole processes

The existence of dynamic processes in the borehole (e.g. pressure fluctuations caused by DRPs) is well-known for many years.[32,33] However, only now with the rise of fully monitored LWD technology they can also be brought into context to borehole breakouts. Meng et al. (2019)[58] emphasized the need for the consideration of dynamic hydraulic conditions in the borehole by numerical and experimental analyses highlighting the influence of these conditions on borehole stability.

The analyses of 208 breakout datasets, presented herein, highlight the possible impact of dynamic processes. This first investigation already enables a statistical assessment that should
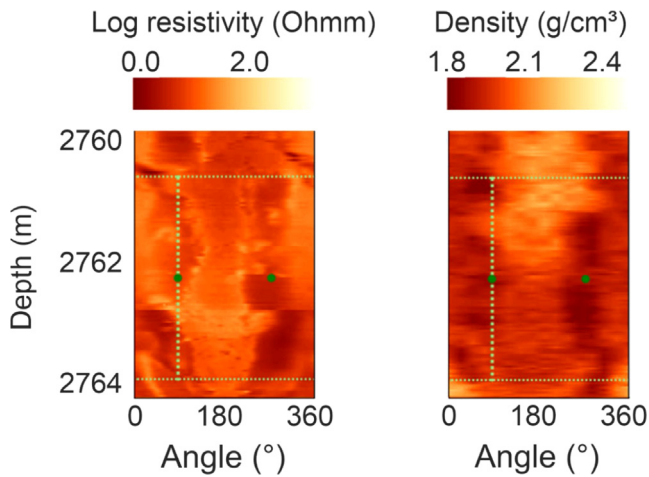
Fig. 8. Temporal geometrical changes of a breakout from a BHA with multiple imaging tools: a resistivity image with ∼16 m offset to the bit (left) and a density image with ∼31 m offset to the bit (right).

be further refined in the future. We observed strong pressure fluctuations of up to 16 % of the absolute annulus pressure in the open-hole sections occurring within minutes after being drilled (Fig. 5). There are clear indications that they have been caused by DRPs, most prominently by pump shut-off events. These pressure changes consequently result in fluctuations in the effective circumferential stress around the borehole leading to possible rock failure (i.e. breakouts). Our results further show that these pressure (and subsequent stress) fluctuations occur in almost every investigated breakout section. This points out the need of controlling such pressure fluctuations in well operations for improving wellbore stability.

4.2. Temporal development of borehole breakouts

The exemplary result in chapter 3.4 (Fig. 7) shows that breakouts may grow in both length and opening angle. When a BHA contains multiple imaging tools that are installed at different offsets to the bit, it will acquire images at different times after the formation has been drilled. This opens the pathway to analyzing breakout geometries at different acquisition times in addition to utilizing relogs. Fig. 8 shows the recording of such a BHA having both, a resistivity and a density image tool, with offsets to the bit of 16 and 31 m, respectively. It can be seen that the breakout appears to widen slightly in the density image with a more pronounced shape, especially in the upper part of the breakout, which is only indicated in the resistivity image. Additionally, the different depth of investigation (DOI) of the two tools has to be considered. Whereas the resistivity image has a DOI of ca. 0.5 in, representing a breakout width directly at the borehole wall, the density image reading is related to a DOI of ca. 3.5 in. This results in an underestimation of the breakout width in the density image. Thus, it can be concluded that the breakout width grew significantly over time between the acquisitions of the two images.

A similar analysis approach was described by Moore et al. (2011)[23] evaluating changes in breakout width between two different images in the same BHA observed under constant hydraulic conditions. In contrast to these findings, the breakout development shown in Fig. 8 was influenced by pressure fluctuations due to a connection, which was performed during the acquisition of the resistivity image (closer to the bit). Hence, the annulus pressure was reduced by approximately 1.5 MPa. The connection, however, was already finished before the density image was recorded. This succession may lead to the conclusion that the borehole conditions captured by the density image were more strongly influenced by the connection than at the time when the resistivity image was acquired. These differences are especially prevalent in the shallower part of the images: the breakout is only slightly indicated in the resistivity image, whereas it is visible in the density image.

This observation over time may also explain earlier studies of the temporal development of breakouts.[23,59] It illustrates the influence of dynamic conditions on breakout development. It also has consequences for the derivation of far-field stress magnitudes as they are directly related to the breakout width.[9]

5. Conclusions

Our investigation provides a clear correlation between the occurrence of borehole breakouts and DRPs exists, mostly due to connections and tripping operations. When major DRP activities took place in a specific borehole interval, it also exhibits a strong breakout signature. The fact that in breakout sections, DRPs were conducted ten times more often than in other drilling sections points to a causal relationship between the drilling activity and the origin of breakouts. It is therefore suggested that their occurrence not only depends on rock strength and the naturally occurring stress state already beyond the yield envelope but also on drilling activities leading to an effective stress state beyond failure. This concept could only be obtained using modern LWD technology with real-time drilling data acquisition – traditional wireline logging would not allow for this observation. It has the potential to lead to novel breakout analyses.

DRPs have also a significant impact on the conditions within and around a borehole. This includes the pressure and temperature fields as well as mechanical rock properties. Frequent dynamic changes in pressure and temperature at the bottom hole may serve as a proxy for breakouts. We observed that dynamic drilling-induced pressure changes may directly contribute to wellbore failure. Especially pump shut-off events (e.g. during connections) could be related to significant pressure drop anomalies of up to 16% of the average annulus pressure.

These findings can also support decision processes to secure borehole stability. They demonstrate the necessity to control the downhole pressure to prevent changes in the effective stresses around a well. When an unexpected pressure change is observed, possible countermeasures such as mud weight adaptation should be taken. Alternatively, a larger safety margin on the pre-drilling pressure window could be applied. In contrast to these preventive measures, actively initiated pressure changes and related perturbations of the effective stress can cause wellbore instabilities in specific sections. DRPs could also influence the occurrence of tensile fractures (i.e. DIFs or hydraulic fractures parallel to S_{max}) or compressive borehole breakouts (i.e. parallel to S_{min}). The results of this study show that drilling can accidentally stimulate a borehole and future drilling operations have to be adapted.

In terms of research on mechanical behavior, relogs of breakout intervals open the perspective of investigating the time-dependency of breakouts and the influence of DRPs thereof. Our analysis shows that breakouts may tend to grow both azimuthally and in the measured depth direction, confirming the findings published earlier.

It adds an important component for geomechanical analyses when using the azimuthal width of breakouts to determine the magnitude of the maximum horizontal stress. We could further show that running a BHA with different image tools additionally enables us to investigate time-dependent borehole failure and to show the direct impact of DRPs on breakout growth.

The data used in this study only rarely included abundant relog sections or multiple images with sufficient quality. In a

thorough investigation, this data basis should be improved to better quantify the causality of the relationship between DRPs and the occurrence of breakouts. For this purpose, future research should focus on clarifying this causality between DRPs and breakouts. This could be realized by comparing two nearby boreholes with one having previously performed DRPs and the other rather avoiding it in similar depths.

CRediT authorship contribution statement

Kai Stricker: Methodology, Software, Formal analysis, Investigation, Writing – original draft, Visualization. **Stefan Schimschal:** Conceptualization, Software, Methodology, Writing – review & editing. **Birgit Müller:** Writing – review & editing, Supervision. **Stefan Wessling:** Conceptualization, Writing – review & editing, Supervision, Project administration, Funding acquisition. **Florian Bender:** Writing – original draft, Writing – review & editing. **Thomas Kohl:** Writing – review & editing, Supervision.

Declaration of competing interest

The authors declare that they have no known competing financial interests or personal relationships that could have appeared to influence the work reported in this paper.

Data availability

All analyzed non-confidential data was uploaded to a repository (https://data.mendeley.com/datasets/r3tb2bdr7s). Non-confidential raw data can be obtained from https://www.npd.no/en/diskos/wells/.

References

1. Steiger Ronald P, Leung Peter K. Quantitative determination of the mechanical properties of shales. *SPE Drill Eng.* 1992;7(03):181–185. http://dx.doi.org/10.2118/18024-PA.
2. Wessling Stefan, Bartetzko Anne, Pei Jianyong, Dahl Thomas. Automation in wellbore stability workflows. In: *SPE Intelligent Energy International.* SPE; 2012.
3. Albukhari TM, Beshish GK, Abouzbeda MM, Madi A. Geomechanical wellbore stability analysis for the reservoir section in JNC186 oil field. In: Hamdi E, ed. *ISRM 1st International Conference on Advances in Rock Mechanics - Tunirock 2018.* 2018:179–193.
4. Ashena R, Elmgerbi A, Rasouli V, Ghalambor A, Rabiei M, Bahrami A. Severe wellbore instability in a complex lithology formation necessitating casing while drilling and continuous circulation system. *J Petrol Explor Prod Technol.* 2020;10(4):1511–1532. http://dx.doi.org/10.1007/s13202-020-00834-3.
5. Zoback Mark D. *Reservoir Geomechanics.* Cambridge University Press; 2007.
6. Brudy Martin, Kjorholt Halvor. Stress orientation on the Norwegian continental shelf derived from borehole failures observed in high-resolution borehole imaging logs. *Tectonophysics.* 1992;337:65–84.
7. Bell JS. In situ stresses in sedimentary rocks: Measurement techniques. *Geosci Can.* 1996;23(2):85–100.
8. Tingay M, Reinecker J, Müller BIR. Borehole breakout and drilling-induced fracture analysis from image logs. 2008 World Stress Map Project Guidelines: Image Logs.
9. Barton CA, Zoback Mark D, Burns L. In-situ stress orientation and magnitude at the Fenton Geothermal Site, New Mexico, determined from wellbore breakouts. *Geophys Res Lett.* 1988;15(5):467–470. http://dx.doi.org/10.1029/gl015i005p00467.
10. Moos Daniel, Zoback Mark D. Utilization of observations of well bore failure to constrain the orientation and magnitude of crustal stresses: application to continental, Deep Sea Drilling Project, and Ocean Drilling Program boreholes. *J Geophys Res Solid Earth.* 1990;95(B6):9305–9325.
11. Aadnoy Bernt S, Bell JS, et al. Classification of drilling-induced fractures and their relationship to in-situ stress directions. *Log Anal.* 1998;39(06).
12. Gaillot Philippe, Brewer Tim, Pezard Philippe, Yeh En-Chao. Borehole imaging tools - Principles and applications. *Sci Drill.* 2007;5. http://dx.doi.org/10.2204/iodp.sd.5.07s1.2007.
13. Li Q, Bornemann T, Rasmus J, Wang H, Hodenfield K, Lovell J. Real-time logging-while-drilling image: Techniques and applications. In: *SPWLA 42nd Annual Logging Symposium.* SPWLA; 2001.
14. Tollefsen E, Weber A, Kramer A, Sirkin G, Hartman D, Grant L. Logging while drilling measurements: From correlation to evaluation. In: *International Oil Conference and Exhibition.* SPE; 2007.
15. Wessling Stefan, Dahl Thomas, Pantic Dinah. Challenges and solutions for automated wellbore status monitoring - Breakout detection as an example. In: *SPE Digital Energy Conference and Exhibition.* SPE; 2011.
16. Hillis RR, Reynolds SD. The Australian stress map. *J Geol Soc.* 2000;157(5):915–921.
17. Peška Pavel, Zoback Mark D. Compressive and tensile failure of inclined well bores and determination of in situ stress and rock strength. *J Geophys Res Solid Earth.* 1995;100(B7):12791–12811.
18. Kristiansen TG. Drilling wellbore stability in the compacting and subsiding Valhall field. In: *IADC/SPE Drilling Conference 2004.* Society of Petroleum Engineers; 2004.
19. Zeynali ME. Mechanical and physico-chemical aspects of wellbore stability during drilling operations. *J Pet Sci Eng.* 2012;82–83:120–124. http://dx.doi.org/10.1016/j.petrol.2012.01.006.
20. AlBahrani H, Morita N. Understanding the concurrence of drilling induced fractures and breakouts and its implications on drilling performance using a 3D FEM and field imaging data. In: *International Petroleum Technology Conference.* 2020.
21. Gallant C, Zhang J, Wolfe C, Freeman J, Al-Bazali T, Reese M. Wellbore stability considerations for drilling high-angle wells through finely laminated shale: A case study from Terra Nova. In: *SPE Annual Technical Conference and Exhibition.* SPE; 2007.
22. Hayavi Mohammad Tabaeh, Abdideh Mohammad. Determination of safe mud pressure window for different well trajectories and stress regimes during drilling operations. *Geomech Energy Environ.* 2017;12:14–20. http://dx.doi.org/10.1016/j.gete.2017.07.002.
23. Moore J, Chang C, McNeill L, Thu MK, Yamada Y, Huftile G. Growth of borehole breakouts with time after drilling: Implications for state of stress, NanTroSEIZE transect, SW Japan. *Geochem Geophys Geosyst.* 2011;12(4):1–15. http://dx.doi.org/10.1029/2010gc003417.
24. Schoenball M, Sahara DP, Kohl T. Time-dependent brittle creep as a mechanism for time-delayed wellbore failure. *Int J Rock Mech Min Sci.* 2014;70:400–406. http://dx.doi.org/10.1016/j.ijrmms.2014.05.012.
25. Jaeger JC, Cook Neville GW, Zimmerman Robert W. *Fundamentals of Rock Mechanics.* 4th ed. Malden, MA: Blackwell Publ.; 2007 Available online at http://www.loc.gov/catdir/enhancements/fy0802/2006036480-b.html.
26. Colmenares LB, Zoback MD. A statistical evaluation of intact rock failure criteria constrained by polyaxial test data for five different rocks. *Int J Rock Mech Min Sci.* 2002;39(6):695–729. http://dx.doi.org/10.1016/S1365-1609(02)00048-5.
27. Kirsch C. Die Theorie der Elastizität und die Bedürfnisse der Festigkeitslehre. *Z Vereines Deutscher Ingenieure.* 1898;42:797–807.
28. Bergant A, Simpson AR, Tijsseling AS. Water hammer with column separation: A historical review. *J Fluids Struct.* 2006;22(2):135–171. http://dx.doi.org/10.1016/j.jfluidstructs.2005.08.008.
29. Yang JH, Jiang QH, Zhang QB, Zhao J. Dynamic stress adjustment and rock damage during blasting excavation in a deep-buried circular tunnel. *Tunn Undergr Space Technol.* 2018;71:591–604. http://dx.doi.org/10.1016/j.tust.2017.10.010.
30. SOG. Schlumberger oilfield glossary. 2022 Available online at https://glossary.oilfield.slb.com/.
31. Bagala S, McWilliam I, O'Rourke T, Liu C. Real - Time geomechanics: Applications to deepwater drilling. In: *SPE Deepwater Drilling and Completions Conference, Vol. 137071.* SPE; 2010.
32. Lake Larry. *Petroleum Engineering HandBook.* Richardson, TX: Society of Petroleum Engineers; 2006.
33. Burkhardt JA. Wellbore pressure surges produced by pipe movement. *J Pet Technol.* 1961;13(06):595–605. http://dx.doi.org/10.2118/1546-G-PA.
34. Dupriest FE, Elks WC, Ottesen S, Pastusek PE, Zook JR, Aphale CR. Borehole quality design and pracices to maximize drill rate performance. In: *SPE Annual Technical Conference and Exhibition, Vol. 134580.* SPE; 2010.

35. NPD. *The Norwegian National Data Repository for Petroleum Data. Diskos Well Database.* Norwegian Petroleum Directorate; 2022 Available online at https://www.npd.no/en/diskos/wells/, checked on 12/8/2022.

36. Stricker Kai, Schimschal Stefan, Wessling Stefan, Müller BIR, Bender Florian, Kohl Thomas. LWD breakout data from hydrocarbon fields in the Norwegian North Sea, Mendeley Data, V1; 2022. http://dx.doi.org/10.17632/r3tb2bdr7s.1.

37. Johnsen Jan R, Rutledal Helge, Nilsen Dag Erik. Jurassic reservoirs; field examples from the oseberg and Troll fields: Horda platform area. In: *Petroleum Exploration and Exploitation in Norway - Proceedings of the Norwegian Petroleum Society Conference, Vol. 4.* Elsevier; 1995:199–234 (Norwegian Petroleum Society Special Publications).

38. Løseth Tore M, Ryseth Alf E, Young Mike. Sedimentology and sequence stratigraphy of the middle Jurassic Tarbert Formation, Oseberg South Area (Northern North Sea). *Basin Res.* 2009;21(5):597–619. http://dx.doi.org/10.1111/j.1365-2117.2009.00421.x.

39. Ceccato Alberto, Viola Giulio, Tartaglia Giulia, Antonellini Marco. In–situ quantification of mechanical and permeability properties on outcrop analogues of offshore fractured and weathered crystalline basement: Examples from the Rolvsnes granodiorite, Bømlo, Norway. *Mar Pet Geol.* 2021;124:104859. http://dx.doi.org/10.1016/j.marpetgeo.2020.104859.

40. Bretan Peter, Yielding Graham, Mathiassen Odd Magne, Thorsnes Tove. Fault-seal analysis for CO 2 storage: an example from the troll area, Norwegian continental shelf. *PG.* 2011;17(2):181–192. http://dx.doi.org/10.1144/1354-079310-025.

41. Holgate Nicholas E, Jackson Christopher A-L, Hampson Gary J, Dreyer Tom. Sedimentology and sequence stratigraphy of the Middle–Upper Jurassic Krossfjord and Fensfjord formations, Troll Field, northern North Sea. *PG.* 2013;19(3):237–258. http://dx.doi.org/10.1144/petgeo2012-039.

42. Munns JW. The Valhall field: a geological overview. *Mar Pet Geol.* 1985;2(1):23–43. http://dx.doi.org/10.1016/0264-8172(85)90046-7.

43. Zoback Mark D, Zinke Jens C. Production-induced normal faulting in the Valhall and Ekofisk oil fields. In: Trifu Cezar I, ed. *The Mechanism of Induced Seismicity.* Basel: Birkhäuser Basel; 2002:403–420.

44. Kristiansen TG, Plischke B. History matched full field geomechanics model of the Valhall field including water weakening and re-pressurisation. In: *SPE EUROPEC/EAGE Annual Conference and Exhibition.* 2010.

45. Ellis Darwin, Singer Julian. *Well Logging for Earth Scientists.* Dordrecht London: Springer; 2007.

46. Lindsay G, Ong S, Morris S, Lofts J. Wellbore stress indicators while drilling: A comparison of induced features from wireline and LWD high-resolution electrical images. In: *SPE/IADC Drilling Conference and Exhibition 2007.* SPE; 2007.

47. Fulda Christian, Hartmann Andreas, Gorek Matthias. High resolution electrical imaging while drilling. In: *SPWLA 51st Annual Logging Symposium.* SPWLA; 2010.

48. Gillen ME, Moody B, Dymmock S. New LWD technology provides high-resolution images in oil- and water-based muds for improved decision making in real time. In: *Offshore Technology Conference.* 2018.

49. Meyer Nicolas, Holehouse Steve, Kirkwood Andrew, et al. Improved LWD density images and their handling for thin bed definition and for hole shape visualization. In: *SPWLA 46th Annual Logging Symposium.* SPWLA; 2005.

50. Ekstrom MP, Dahan CA, Chen MY, Lloyd PM, Rossi DJ. Formation imaging with microelectrical scanning arrays. *Log Anal.* 1987;28:294–306.

51. Evans D, Graham C, Armour A, Bathurst P. *The Millenium Atlas: Petroleum Geology of the Central and Northern North Sea.* London: The Geological Society of London; 2003.

52. Gradstein Felix M, Anthonissen Erik, Brunstad Harald, et al. Norwegian Offshore Stratigraphic Lexicon (NORLEX). *NoS.* 2010;44(1):73–86. http://dx.doi.org/10.1127/0078-0421/2010/0005.

53. Thompson N, Andrews JS, Reitan H, Rodrigues NET. Data mining of in-situ stress database towards development of regional and global stress trends and pore pressure relationships. In: *SPE Norway Subsurface Conference.* Society of Petroleum Engineers; 2022.

54. Hillis RR, Nelson EJ. In situ stresses in the North Sea and their applications: petroleum geomechanics from exploration to development. In: Doré AG, Vining BA, eds. *6th Petroleum Geology Conference. Petroleum Geology: North-West Europe and Global Perspectives. Petroleum Geology Conference.* London: Geological Society; 2005:551–564.

55. Alizadeh M, Movahed Z, Junin R, Mohsin R. Finding the drilling induced fractures and borehole breakouts directions using image logs. *J Adv Res Appl Mech.* 2015;10(1):9–30.

56. Li Xiaorong, El Mohtar Chadi S, Gray KE. Modeling progressive wellbore breakouts with dynamic wellbore hydraulics. *SPE J.* 2020;25(02):541–557. http://dx.doi.org/10.2118/199887-PA.

57. AlBahrani H, Al-Qahtani A, Marhoon Z, Hamid O. A newly developed process for wellbore geometry analysis from a geomechanical perspective. In: *SPE Kingdom of Saudi Arabia Annual Technical Symposium and Exhibition, 192210-MS. SPE Kingdom of Saudi Arabia Annual Technical Symposium and Exhibition.* SPE; 2018.

58. Meng Meng, Zamanipour Zahra, Miska Stefan, Yu Mengjiao, Ozbayoglu EM. Dynamic wellbore stability analysis under tripping operations. *Rock Mech Rock Eng.* 2019;52(9):3063–3083. http://dx.doi.org/10.1007/s00603-019-01745-4.

59. Azzola Jérôme, Valley Benoît, Schmittbuhl Jean, Genter Albert. Stress characterization and temporal evolution of borehole failure at the Rittershoffen geothermal project. *Solid Earth.* 2019;10(4):1155–1180. http://dx.doi.org/10.5194/se-10-1155-2019.